JOURNAL OF MATERIALS SCIENCE **36** (2001) 3119–3128

Drawability and attainable mechanical properties of polyamide yarn using true stress–true strain curves

J. VAN RUITEN, R. RIEDEL, R. DEBLIECK*, R. BROUWER, J. P. PENNING
Centre for Fibre Technology, DSM Research, PO BOX 18, 6160 MD Geleen, The Netherlands
E-mail: jippe.ruiten-van@dsm.com

The present paper applies the concept of a molecular network to the analysis of melt spun Polyamide 4.6 fibres (Stanyl® from DSM, The Netherlands), obtained at different wind up speeds, and the yarns, subsequently drawn from these. The mechanical properties of the yarns produced are discussed in terms of the network draw ratio, determined by matching true stress–true strain curves. It is shown that analysis of true stress–true strain curves of as-spun yarns of different orientation, can be used to predict their drawability (final tenacity versus draw ratio). Moreover, the maximum attainable tenacity of drawn yarns under given drawing conditions can be forecasted. It is shown that the Edwards–Vilgis rubber elastic model is able to describe the network deformational behaviour of the as-spun yarns over a wide range of draw ratios. The apparent network draw ratio, obtained by curve matching the drawn yarn true stress–true strain curves with those of its precursor yarn, shows discrepancies with the actually applied draw ratio in the drawing process. These discrepancies are discussed in terms of network structural parameters. It is made plausible that growth of existing crystals during hot-drawing is responsible for this, rather than formation of new crystals.

1. Introduction

From a yarn producers point of view it is of particular practical relevance to optimise yarn production processes. The objective for technical yarns is to obtain the highest mechanical properties in the shortest of process. Ultimately, it would be desirable to obtain fully oriented structures approaching theoretical maximum properties by simply spinning at high take-up speeds. It is well known that this has not been realised up till now, and a (separate) drawing process is necessary to obtain the desired property balance of tenacity, elongation to break and shrinkage for technical yarns. There is however an important trade-off between the structure of the as-spun yarns (Low Oriented Yarns, LOY, or Partially Oriented Yarns, POY) after spinning and the subsequently required drawing process. In other words, take-up speed in the spinning process is an important process variable influencing the drawn yarn (denoted by FDY or Fully Drawn Yarn) properties, as well as production economics. Control over the relation is important, both from a practical as well as a scientific point of view.

In earlier work of Ward *et al*. [1–4], the mechanical behaviour of PET yarns of different take-up speed and/or draw ratio has been rationalised in terms of a network deformation model. In this approach, a molecular network is supposed to develop in the polymer in the spinning thread line, and is assumed to deform according to rubber network elasticity theory upon stretching. Crucial to the approach is the assumption that the network retains its nature in the course of further processing, such as drawing or heat setting. This approach allows to link and mutually compare several yarn production processes to each other and compare yarns of very different origin on a one to one basis.

The merits and limitations of the molecular network concept have been elucidated in a number of publications, mainly for PET yarns. Pinnock and Ward [1] successfully represented the molecular structure of melt spun PET fibres by such a molecular network. Allison *et al*. [2] used the network concept in a drawability study on PET fibres and showed that the extension of the network was partitioned between the stretch produced in the spinning thread line and the subsequent cold drawing step. The higher the take-up speed during spinning, the greater the network extension of the as-spun yarn, and the lower the subsequent extensibility on cold drawing.

The development of high-speed spinning processes has required modification of the network concept. Heuvel and Huisman [5] showed that at high take-up speeds, besides deformation of the network, crystallisation occurs in the spinning thread line. It was shown by Ward and collaborators [3, 4] that, to a first

* *Present Address*: Dutch Polymer Institute, The Netherlands.

approximation, the induced crystallisation in the spinning thread line at higher take-up speeds (for the studied PET typical degrees of crystallisation were around 25%) did not change the network topology appreciably, since properties such as birefringence and elastic modulus were shown to correlate well with the network draw ratio λ_{net}, obtained by shifting true stress–true strain curves. Shirataki *et al*. [6] reached similar conclusions. They also found that fracture properties were consistent with the constant network assumption, implying the existence of a (network) unique limiting draw ratio, irrespective of initial molecular orientation or crystallinity. For PET a limiting network draw ratio around 10 was obtained.

Although the concept of a molecular network in analysing drawability of man-made fibres has been well developed for PET fibres, very few studies have addressed this issue for other polymers, such as for instance polyamides, although they are technically as well as commercially important fibre polymers.

The present study aims at applying the concept of a molecular network to the analysis of melt spun Polyamide 4,6 fibres (Stanyl® from DSM, The Netherlands), obtained at different wind up speeds, and the yarns, subsequently hot-drawn from these. One of the important goals is to show the validity of the constant network topology concept for Polyamide 4,6 yarns, and demonstrate its merit in predicting the drawability (final tenacity versus draw ratio) of the fully drawn yarns. Moreover, a method is presented which enables one to forecast the maximum attainable tenacity of drawn yarns under given drawing conditions, from the mechanical properties of their precursor.

2. Experimental

2.1. Material and methods

Polyamide 4,6 (PA4,6) produced by DSM in the Netherlands under the trade name Stanyl® was used in this study. It is prepared by polycondensation of 1,4-diaminobutane and adipic acid. In order to enable melt processing, filament formation and drawability, the Stanyl® fibre grade contains 5% comonomer. In the whole range of aliphatic polyamides, PA4,6 stands out because of its high melting point and its high degree of crystallinity. Compared to PA 6 or PA6,6, the PA4,6 chemical structure is characterised by a higher concentration of amide linkages and a higher (point) symmetry along the chain axis. Furthermore the regularity along the chain is higher, since the distance between two amide linkages in PA4,6 is the same (4 methylene groups) in the diamine and diacid unit. This higher chain regularity is the basis for the higher crystallisation rate, the higher melting point (283°C) and the higher crystallinity of PA4,6, compared to other polyamides. In yarn properties, Stanyl® PA4,6 discriminates itself with a considerably higher modulus at elevated temperatures, a much higher shrinkage force at equal or lower shrinkage, and much lower creep, compared to other polyamides.

Stanyl® as-spun yarns were produced on lab scale spinning equipment at take-up speeds ranging from 500 m/min to 4200 m/min. The as-spun yarns were hot drawn on an Erdmann Drawmod drawing frame over three godets. The godets temperatures were 120°C, 220°C and room temperature. A hot contact plate was used between the first two godets; its temperature was 195°C. Draw ratios varied between 3.5 and 5.1. Tensile tests on all yarns were performed on a Statimat tensile tester with a gauge length of 100 mm and at an extension rate of 1 min^{-1}.

Birefringence values were obtained with a polarizing microscope and Quartz-compensator. Density measurements to obtain yarn crystallinity were carried out using a CCl_4/heptane density gradient column.

2.2. Obtaining network draw ratio using true stress–true strain data

The network extension produced during the spinning operation can for amorphous PET be obtained by measuring the shrinkage of the as-spun yarn (recovered strain in boiling water) [2]. However this procedure is no longer valid when crystallisation has occurred in the spinning thread line since the formed crystals prevent recovery of frozen-in strains. Indeed, crystallisation causes a fixation of the network in its post-spinning extended form, which is apparent from a gradual reduction in as-spun boiling water shrinkage with take-up speed. Brody [7] therefore designed a procedure to evaluate network extensibility on a relative basis. He measured true stress–true strain (TSTS) curves at room temperature (in fact a process of cold drawing) of yarns, spun at different take-up speed, and found that these curves could be shifted a certain amount over the log (λ) axis (λ being the extension ratio), such that their final parts perfectly coincided. The shift for a certain take-up speed, produced relative to the TSTS curve for the lowest take-up speed, is thus assumed to be the cold draw, equivalent to the network extension (draw ratio), resulting from spinning at this take-up speed, and relative to the lowest take-up speed spinning process.

Under the assumptions of constant volume (or density) and homogeneous deformation during tensile drawing, true stresses and strains can simply be obtained from nominal stress and conventional strain by the following formulae:

$$\sigma_{true} = \sigma_{nom}{}^{*}\lambda \tag{1}$$

$$\lambda = l/l_0 = \varepsilon + 1 \tag{2}$$

where σ_{true}, σ_{nom}, λ, l, l_0, and ε are true stress, nominal stress (force divided by original cross-section), draw ratio, actual length, original length and conventional strain respectively. Only when the network extension in the fibre spun at the lowest take-up speed is zero (no network orientation), network draw ratios obtained on fibres at higher take-up speed by the shifting procedure become absolute. We will reserve the term True Strain to quantify absolute draw ratio, i.e. for those situations where the samples are isotropic at $\lambda_{true} = 1$. In order to obtain accurate network draw ratios it is therefore important to know the network orientation of the reference as-spun fibre. This 'reference' orientation was obtained by measuring birefringence, as is explained below.

A similar approach—shifting of TSTS curves—can be used to determine the network draw ratio for a series of hot drawn yarns with respect to their precursor. At any stage in the process the total network draw ratio is the product of all prior imposed draw ratios. Using true stress data, one can not only compare in an equal way yarns of different yarn count, but also in different stages of drawing during the tensile test. Adopting the idea that mechanical properties may be dominated by the extent of deformation (orientation) of the virtual network, one can thus start to look for differences and similarities between yarns of different origin. Moreover rationalisation of the differences in this manner may help to understand the reasons why mechanical response is different, and how they may be influenced in the spinning and drawing stage.

Adding network orientation can be done in several consecutive steps, such as spinning, hot drawing and tensile testing. The total draw ratio of a sample after having undergone these consecutive drawing steps, can be calculated from the product of draw ratios of the consisting steps. For this reason, true stress–draw ratio plots are made on a logarithmic draw ratio scale. In this way, a different amount of orientation causes just a shift along the ln (λ) scale. Curve matching can therefore be used to determine differences in network orientation. In as-spun LOY yarns, where necking may occur during tensile testing, curve matching can obviously only be done on the homogeneous final part of the true stress–true strain curve at high stresses.

3. Results and discussion

3.1. As-spun yarns at different wind-up speeds

Fig. 1 shows a number of nominal stress-elongation curves for a series of as–spun yarns, produced at wind-up speeds of 500–4200 m/min. Nominal breaking stresses rise considerably with wind-up speed at the expense of ultimate elongation. Although a stiffer behaviour is observed for the higher take-up speed yarns, it is difficult to quantify and compare the differences in (ultimate) mechanical properties of the produced yarns, since their elongation at break differs so widely.

In Fig. 2 the same data have been transformed into true stress–strain (or extension ratio λ) data, using Equations 1 and 2. Again, stiffer behaviour with increasing wind up speed is observed as a result of increasing network orientation in the as-spun yarn. True tenacities now fall within a relatively narrow range of 500–700 MPa for all as-spun yarns. This relatively constant true tenacity in cold drawing, independent of take-up speed has also been observed for PET [7]. For PA6 yarns, true strength was found to rise slowly with birefringence of as-spun yarns, but the effect was much smaller than for modulus [8]. The constancy of true strength with take-up speed to a first approximation suggests there exists some limiting network strength for these as-spun PA4,6 yarns.

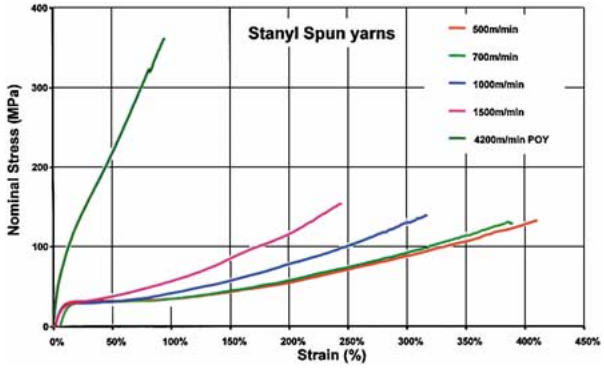

Figure 1 Nominal stress–strain curves of as-spun yarns for different wind-up speeds.

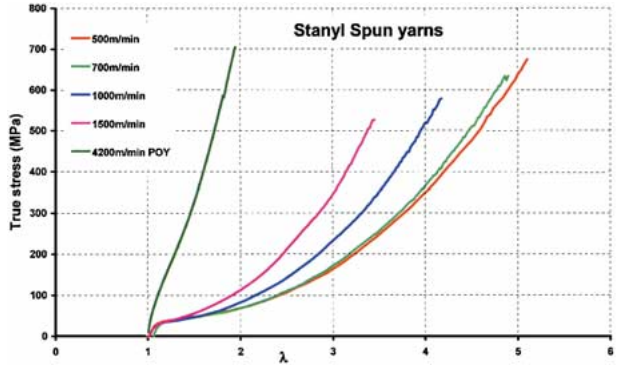

Figure 2 True stress–strain curves of as-spun yarns for different wind-up speeds.

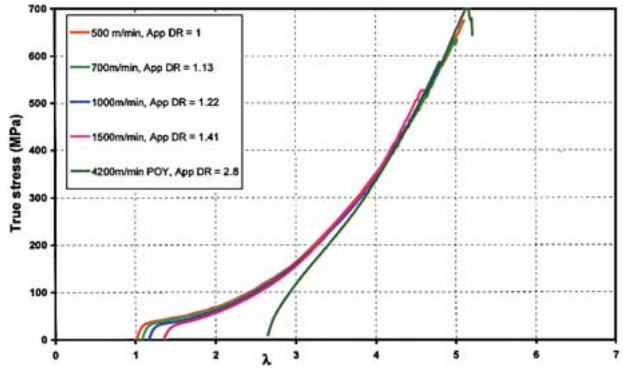

Figure 3 Matched true stress–strain curves of as-spun yarns for different wind-up speeds.

In Fig. 3 the true stress-strain curves have been shifted horizontally (along the ln (λ)-axis) to form a continuous master curve. It can be seen that the curves match rather well, which is indicative of a near identical network topology for all precursor yarns. Interestingly, the true stress-strain curve, obtained on the high speed spun POY yarn (4200 m/min) also matches the master curve remarkably well. This POY yarn shows a network orientation, equivalent to a draw ratio of 2.8, with respect to the lowest take-up speed yarn. The observed excellent superposability of TSTS curves confirms that the total network extensibility, consisting of the combined stretch produced in the spinning thread line and in the cold draw, can be considered constant. Combined with the observation of near constant true tenacity at break, we conclude that the nature of the network in these PA4,6 yarns can be considered to remain constant during the processes of spinning and cold drawing, similar to what has been observed for PET yarns [1–4, 6].

All curves in Fig. 3 have been matched against the lowest orientation as-spun yarn (500 m/min) to obtain

the apparent network draw ratios. In order to obtain absolute network draw ratios against a truly isotropic reference, birefringence measurements on the as-spun yarns of wind-up speed 500–1500 m/min were carried out. These are illustrated in Fig. 4. The non-zero birefringence for the lowest take-up speed yarn at unit apparent draw ratio indicates that this yarn possesses some orientation, and therefore is not a proper isotropic reference. To determine the absolute network draw ratios the birefringence values of the LOY yarns were extrapolated to zero birefringence. The apparent draw ratio corresponding to zero birefringence was then multiplied to all previously determined apparent draw ratios.

The effect of the correction on the true stress-strain curves can be observed in Fig. 5, which represents the absolute composite true stress–true strain curve for all produced as-spun yarns. It is especially important to obtain absolute apparent draw ratios when aiming to describe the yarn mechanical behaviour by rubber elastic models, as is described below. Small offsets in apparent draw ratios greatly affect model parameters, which subsequently become arbitrary and therefore meaningless.

3.2. Fitting the as-spun yarns with rubber elastic models

The as-spun yarn master curve depicted in Fig. 5 has been fitted with several rubber elastic models. Kuhn's classical Gaussian description [9, 10], Ball–Doi–Edwards and Warner's Gaussian description allowing for slippage of entanglement constraints [11], and Edwards–Vilgis's description adding non Gaussian segment statistics to slipping entanglements [12] were used within their appropriate validity ranges. Fitting network models to samples of unknown orientation will yield arbitrary network parameters. The fits were therefore performed on the corrected true stress-strain curves. Ensuring that the network parameters at low strains were identical for all the models checked validity of the fits. The results for the three models are shown in Fig. 6 for the as-spun yarn produced at 500 m/min. The Gaussian model has been used to estimate the low strain network parameters. A yield stress and network modulus of 25.11 MPa and 10.45 MPa respectively were obtained. As it is well known [16], the Gaussian model looses its validity above $\lambda = 3$ and we therefore limited the strain range to approximately 2.5. In order to assess the nature of the network constraints in the Gaussian model, the Ball–Doi–Edwards and Warner (BDEW) description was fitted onto the same TSTS curve using the same strain range. The BDEW model accounts for entanglement contributions, besides the fixed links of the Gaussian model. It features 4 parameters: a corrected yield stress (interpolated to $\lambda = 1$) above which network deformation starts, two network moduli, one due to slipping entanglements (N_s) and the other related to the fixed links (N_c), and a topological parameter (η), describing the ability of an entanglement to slip between fixed links (sliplink mobility). The excess Helmholtz free energy of deformation reads:

$$\frac{F}{kT} = \frac{1}{2} N_c \sum_{i=1}^{3} \lambda_i^2 + \frac{1}{2} N_s \sum_{i=1}^{3} \left[\frac{(1+\eta)\lambda_i^2}{1+\eta\lambda_i^2} + \log\left(1+\eta\lambda_i^2\right) \right]$$

It turns out that fitting the BDEW model leads to values for yield stress and network modulus, which are consistent with the Gaussian result. Moreover the BDEW fit yields zero values for the entanglement modulus. This result implies that the network in the as-spun yarns apparently only features permanent crosslinks. As can be seen from Fig. 6 the BDEW model is not able to describe network deformation over the entire draw ratio range of interest, due to its Gaussian nature. It was therefore attempted to model the deformation by the non-Gaussian Edwards–Vilgis model. Similar to the BDEW model, the Edwards–Vilgis description assumes the

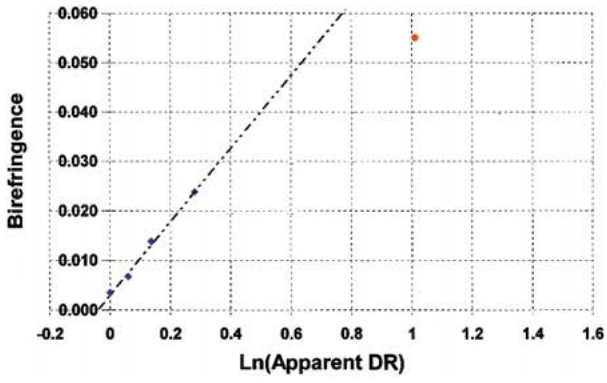

Figure 4 Birefringence vs. ln (apparent network draw ratio) for all as-spun yarns.

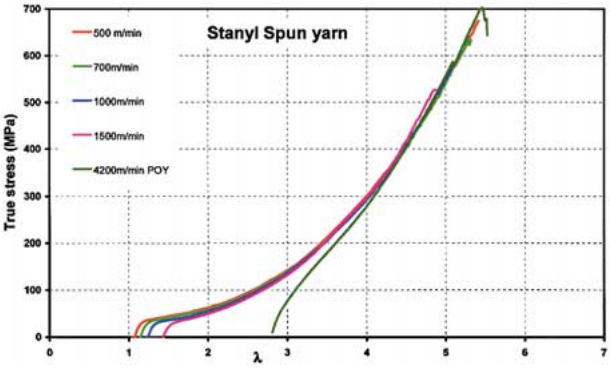

Figure 5 Composite true stress–true strain curve for all as-spun yarns, corrected for off set orientation.

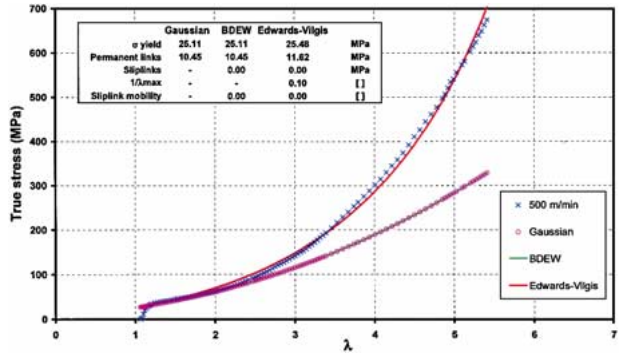

Figure 6 Comparison of rubber elastic model fitting results for the as-spun yarn, produced at 500 m/min.

existence of temporary molecular entanglements in the crosslinked network. The entanglements are modelled as sliplinks. The Edwards–Vilgis theory features 4 parameters in addition to the yield stress: N_c and N_s are the crosslink and sliplink density respectively, while α represents an extensibility parameter ($=1/\lambda_{max}$) and η a measure of the mobility of the temporary sliplinks. If $\eta = 0$, the sliplinks are fixed and will behave as permanent entanglements. The Helmholtz free energy of deformation reads:

$$\frac{F}{kT} = \frac{1}{2}N_c\left[\frac{\sum_{i=1}^{3}(1-\alpha^2)\lambda_i^2}{1-\alpha^2\sum_{i=1}^{1}\lambda_i^2} + \ln\left(1-\alpha^2\sum_{i=1}^{3}\lambda_i^2\right)\right] + \frac{1}{2}N_s\left[\sum_{i=1}^{3}\left\{\frac{\lambda_i^2(1+\eta)(1-\alpha^2)}{\left(1+\eta\lambda_i^2\right)\left(1-\alpha^2\sum_{i=1}^{1}\lambda_i^2\right)} + \ln\left(1+\eta\lambda_i^2\right)\right\} + \ln\left(1-\alpha^2\sum_{i=1}^{3}\lambda_i^2\right)\right]$$

The extensibility parameter accounts for the high strain singularity of non-Gaussian networks. From Fig. 6 it becomes apparent that the Edwards–Vilgis model is the only model able to describe the network behaviour over the total draw ratio range.

The results obtained with the Edwards–Vilgis model confirm the absence of sliplinks. Moreover the network moduli are consistent with the Gaussian and BDEW moduli (11.6 MPa). The fact that sliplinks seem to be absent is consistent with the finding of Hu *et al.* [13]. Based on experimental evidence obtained by NMR, they classified semicrystalline polymers in two classes, "α_c–mobile" and "crystal fixed", depending on the presence or absence, respectively, of a crystalline α-relaxation that provides mobility of chains in and through the crystallites. In 'crystal fixed' polymers, the crystals act as permanent network nodes. From our fitting results it seems that the PA4,6 network response is consistent with this view, whereby the crystallites in the yarns most probably constitute the permanent (crystal fixed) crosslinks in the rubber elastic network. It should be noted that *only* when the model fit is limited to very low draw ratios around 1–2, the BDEW description suggests the presence of some sliplinks. The ability of the Edwards-Vilgis network description to describe the full composite true stress–true strain curve for all as-spun yarns is shown in Fig. 7.

The observed network behaviour for PA4,6 deviates from Edwards–Vilgis rubber elastic modelling results obtained for oriented PET fibre [4]. As-spun PET yarn shows lower crosslink densities than PA4,6. Moreover, the studied PET yarns have sliplinks present at all take-up-speeds, with a higher density of (more mobile) sliplinks at the higher take-up speeds. Important to note here is the fact that PA4,6 yarn, unlike PET, has considerable crystallinity, even at low take-up speed. We will come back to this after discussing the birefringence measurements.

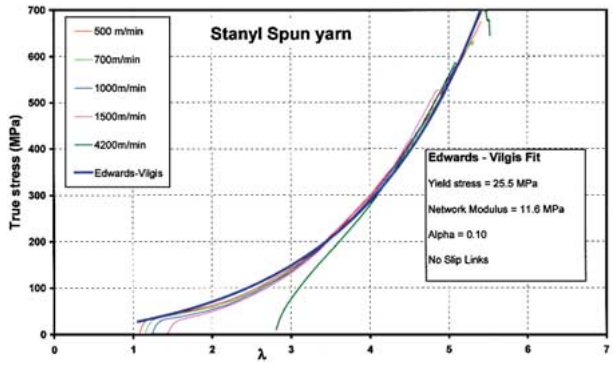

Figure 7 Edwards–Vilgis fitting result for the master TSTS-curve, composed from all as-spun yarns.

3.3. Birefringence results on as-spun and drawn yarns

In order to measure network orientation directly, birefringence measurements were carried out on all as-spun yarns (LOY and POY), as well as on yarns drawn from these precursors. It was observed that birefringence seemed to rise rapidly with apparent draw ratio, levelling off at the higher draw ratios. This behaviour is indicative of a pseudo-affine deformation scheme [14]. For such a scheme the orientation parameter $\langle P_2(\theta)\rangle$ is given by:

$$\langle P_2(\theta)\rangle = \frac{\Delta n}{\Delta n_{max}} = \frac{1}{2}\left[\frac{2\lambda^3+1}{\lambda^3-1} - \frac{3\lambda^3}{(\lambda^3-1)^{3/2}}Arc\ \tan\left((\lambda^3-1)^{1/2}\right)\right]$$

Fig. 8 shows the obtained birefringence values for all yarns against $\langle P_2(\theta)\rangle$. An excellent fit is obtained over the whole range of apparent draw ratios. The maximum birefringence Δn_{max} inferred from the data for PA4,6 is about 0.082. Adherence to the pseudo-affine deformation scheme is not consistent with data obtained on PET yarns, which for as-spun yarns conform to an affine deformation mode, where birefringence is seen to increase rather slowly with network draw ratio [1, 2, 5].

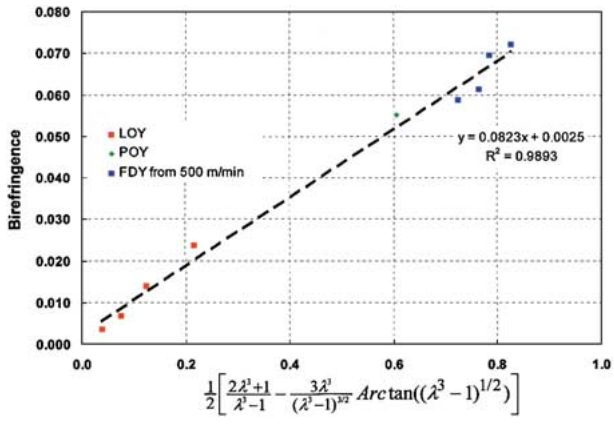

Figure 8 Birefringence vs. orientation parameter $\langle P_2(\theta)\rangle$ for all yarns produced.

The much higher crystallinity of PA4,6 as-spun yarns (around 70%) as compared to typical crystallinity of PET as-spun yarns (0–30%) is responsible for this behaviour.

Indeed, orientation of the crystals increases with take-up speed, because they rotate in order to accommodate the applied deformation. Since the crystals occupy on the average about 70% of the polymer volume, their behaviour makes an important contribution to the overall orientation, as measured by birefringence.

The high crystallinity of as-spun PA4,6 yarns may also explain the unusually high network modulus, found from the Edwards–Vilgis model fit. The tensile network modulus E_{Net} obtained from the model fit is about 12 MPa. Using the relation $M_c = 3\rho RT/E_{\mathrm{Net}}$, and adopting a density of about 1200 kg/m^3, $R = 8.3$ J/K/mol, and $T = 300$ K, an average molecular weight between the network nodes of about 750 g/mol is obtained. At a unit molecular weight of 198 g/mol for a diaminobutane/adipic acid repeat unit, this corresponds to about 3.8 repeat units between the network nodes. This value is unrealisticly low.

The following tentative explanation is offered. The crystals itself are very stiff, and will not directly contribute to any strain. At a typical volume fraction of 70%, the crystals—which constitute the nodes of the assumed virtual network—must have a definite nonzero dimension. Hence, it is evident that the amorphous domains must experience extensive strain magnification. The average local strain experienced by the amorphous network chain parts is therefore factors higher than the macroscopic (true) strain used as ordinate in the TSTS plots. Assuming similar stress levels in amorphous and crystalline domains, this corresponds to locally less stiff behaviour of amorphous domains, and hence a decreased fitted network modulus.

One must add that the assumption of a virtual rubber network may become questionable for highly crystalline polymers, and the studied PA 4,6 in particular, since it is not easy to envisage a network wherein the 'nodes' occupy 70% of the volume. Extracting network parameters from fitting TSTS behaviour may then end up having no meaning at all. On the other hand, the assumption of a network is useful in explaining mechanical behaviour of the PA4,6 yarns, and especially in explaining the effect of increased crystallinity after hot drawing on the measured TSTS behaviour (this is discussed below).

We conclude that the Edwards-Vilgis model describes the behaviour of a network, which is at best *representative* for the actual response. The model parameters do not bare any relation with usual network parameters, but they are used to give insight into observed deviations.

3.4. Comparison of fully drawn yarns at different draw ratios to their precursor LOY

The produced precursor yarns were hot drawn to different draw ratios, ranging from 3.5 to 5.1. The drawn yarns were subsequently subjected to tensile testing at room temperature. In order to validate the concept of network constancy throughout the processes of spinning and hot drawing for the studied PA4,6 yarns, the obtained tensile curves were transformed into TSTS curves and subsequently shifted along the draw ratio axis to match with the (corrected) TSTS curve of the lowest take-up speed LOY yarn. The result of this exercise is represented in Fig. 9.

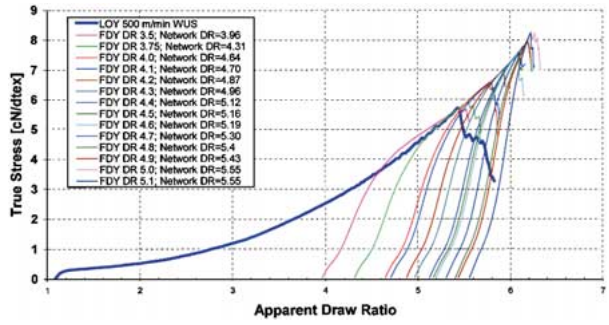

Figure 9 Matched true stress–true strain curves for FDY yarns and the LOY yarn, produced at 500 m/min.

A striking observation from this representation of the results is that the TSTS curve of a drawn yarn consists of two regimes. The first part with the high modulus is most relevant for the actual use of the yarn in the final application. It can be considered as one leg of a kind of hysteretic loop, which becomes apparent when unloading the yarn. Behaviour in this hysteretic regime will strongly depend on the particular conditions that have been set in the relaxation step on the drawing machine. For instance, different behaviour is expected depending on whether the drawn yarns have been subjected to cold or hot relaxation. The second part of the TSTS curve basically follows the network master curve. Apparently the fully drawn yarn "remembers" to which draw ratio it was drawn during hot drawing. If the stress exceeds a certain value, the underlying network will continue to follow this master curve.

The apparent draw ratios obtained by matching the fully drawn yarn TSTS curves with the reference as-spun network curve are plotted in Fig. 10 against the truly applied (total) draw ratio on the drawing frame. To zero order, the apparent draw ratios are remarkably close to the applied deformation (the dotted line in Fig. 10 represents identical draw ratios). This is indicative of the fact that the network topology developed in the as-spun yarns remains fairly constant during

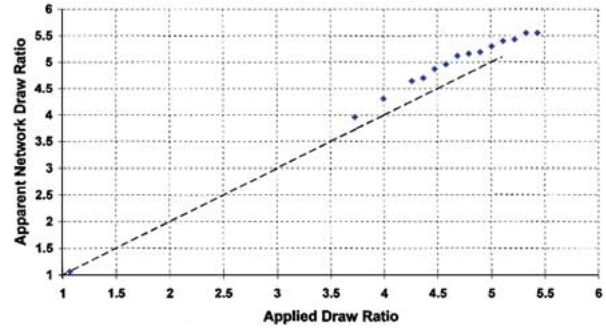

Figure 10 Network draw ratios vs. applied draw ratios for the FDY yarns.

the drawing process, whereby the applied draw ratio is 'transferred' to this constant network.

In the observed good correlation and constancy of the network after drawing, we found justification to assess whether the true stress–true strain curves could be used to predict the drawability and attainable mechanical properties of FDY yarns from the mechanical properties of their precursor. To this end the TSTS properties of a wide variety of LOY yarns, produced under different spinning conditions have been correlated to the mechanical properties of the final FDY yarns drawn from these under identical conditions.

To this end we have, given a reference LOY yarn, quantified the difference in orientation of a new LOY yarn, processed under different conditions, and have correlated this orientation difference, represented by an apparent network draw ratio, to the different draw ratio needed to produce FDY yarns with identical (nominal) tenacity at break. Figs 11–13 illustrate the procedure. In Fig. 11 the TSTS behaviour of two different LOY yarns are compared to each other.

Due to different conditions in the spinning line (higher take-up speed), one LOY yarn shows a stiffer deformation behaviour than the other (reference) yarn. Because of the validity of the constant network assumption, this stiffer behaviour or higher orientation can be quantified by curve matching. In this particular example, the new spinning conditions are equivalent to a network draw ratio difference of 1.105 between the two

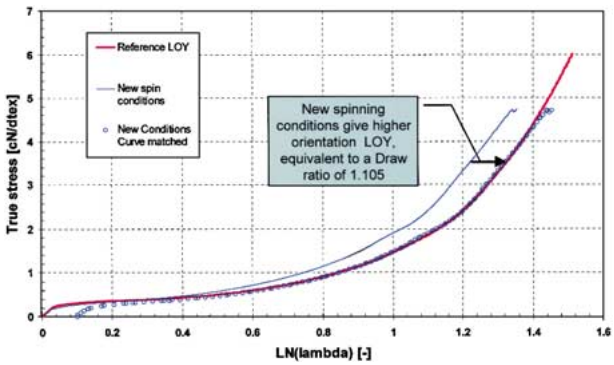

Figure 11 True stress–true strain curves for two LOY yarns with different processing conditions.

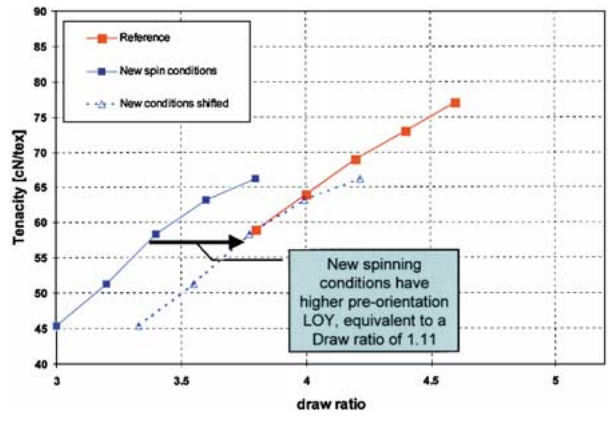

Figure 12 Nominal tenacities of two series of FDY yarns drawn under similar conditions and originating from two LOY yarns with different orientation.

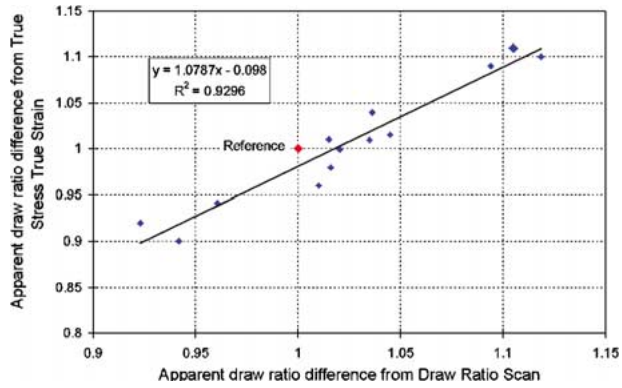

Figure 13 Apparent draw ratio differences from the LOY yarns vs. draw ratio differences from the hot-draw scan.

LOY yarns. The two LOY yarns were subsequently hot drawn under identical conditions at different draw ratios. The obtained nominal tenacities of the two series of produced drawn yarns are depicted in Fig. 12 against the applied draw ratio. The curve on the right belongs to FDY, originating from the reference LOY yarn. The curve on the left corresponds to the LOY yarn with the higher network orientation.

It turns out that shifting horizontally over a draw ratio amount of 1.11 can superpose the two curves. In other words, the FDY yarns produced from the higher orientation precursor LOY, need less draw ratio in the hot drawing stage to attain identical nominal tenacities. The above-described procedure was repeated for a whole series of LOY yarns. In Fig. 13 all apparent draw ratio differences between the different LOY yarns—obtained by shifting their respective TSTS curves—have been plotted against the draw ratio differences, obtained from the draw ratio scan on the drawing machine. The two larger data point markers denote the sample and reference condition depicted in Fig. 12. The fitted line through the data points indicates a slope very close to unity. This result not only means that a higher/lower preorientation in the precursor LOY yarn must be compensated by a lower/higher draw ratio on the hot drawing frame, but moreover that the compensation in draw ratio is equal to the apparent network draw ratio difference. This finding is of considerable practical importance, since it allows establishing a good trend in FDY behaviour on the basis of LOY testing only, rather than going through the full process of drawing and testing of FDY yarns.

The same procedure can also be used to predict differences in attainable FDY tenacities. Whereas Fig. 13 compares the LOY precursor orientation to the orientation needed for production of FDY to obtain the same strain hardening behaviour, a similar correlation can been made between the breaking tenacity of a LOY and the maximum attainable breaking tenacity of the corresponding FDY yarns after drawing. This correlation is given in Fig. 14. The two larger data point markers denote the sample and reference condition depicted in Fig. 12. Again the slope of the fitted straight line is very close to one. It clearly shows that optimisation of the spinning conditions for higher FDY tenacity at break, can be judged directly from the as-spun yarn true tenacity at break.

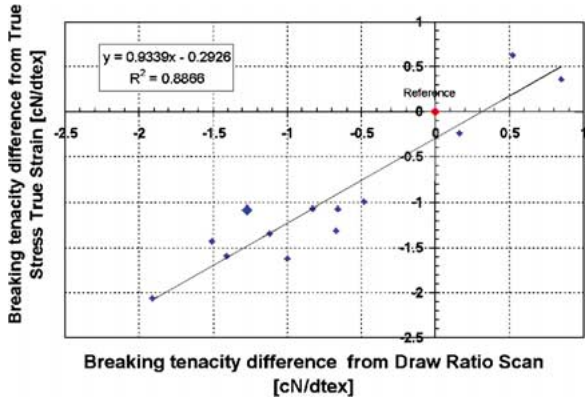

Figure 14 Fracture tenacity differences from the LOY yarns vs. breaking tenacity differences from the hot-draw scan.

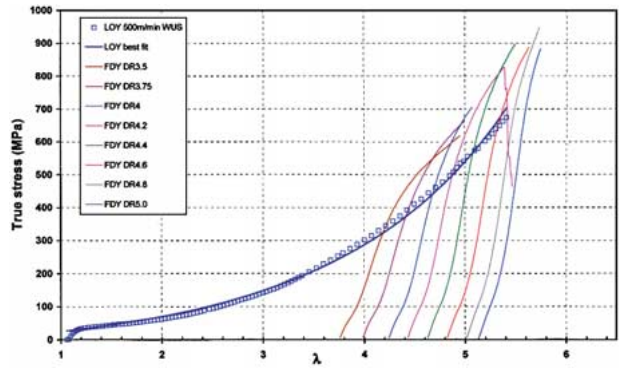

Figure 15 True stress–true strain curves of the FDY yarns, calculated from their final yarn count.

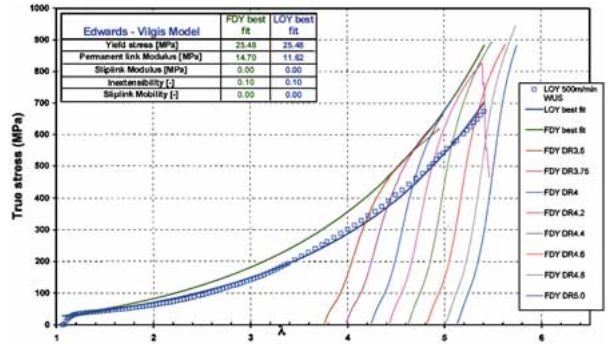

Figure 16 True stress–true strain curves of the FDY yarns, calculated from their final yarn count and fitted with the Edwards–Vilgis network description.

The above results are roughly consistent with the findings of Hotter *et al*.[15]. In a study comparing the properties of several precursor PET yarns, produced at different take-up speed, but drawn/heat set to the same elongation at break, it turned out that tenacity of the drawn yarns was much affected by the take-up speed of the precursor yarn. Nominal tenacity decreased with take-up speed of the precursor yarns, while modulus was seen to increase with precursor take-up speed. Although results were not quantified in terms of network draw ratios, this was explained by a variation in the number and/or the distribution of lengths associated with the tie molecules. Assuming an equal number of tie molecules in the drawn/heat set samples, the observed property variation was explained by an increase in the number of relatively more taut tie molecular chains in the higher take-up speed filaments. The greater number of taut tie molecules would indeed increase initial modulus, while the fewer number of tie chains of average length, which ultimately dictate tenacity, would decrease tenacity.

3.5. Additional strain hardening after hot drawing

A closer look at Fig. 10 shows that the apparent network draw ratios of the hot drawn yarns are consistently above the applied draw ratio. This indicates more strain hardening than one would expect if the network topology would be completely invariant to hot drawing. It is possible to calculate the true strain of the FDY yarns from the ratio of the produced yarn dtex. Doing this will result in a shift of the TSTS curves along the draw ratio axis, with respect to the position of the FDY yarn curves in Fig. 10. Fig. 15 depicts the TSTS curves of the FDY yarns obtained in this way, together with the TSTS curve of the LOY yarn produced at a take-up speed of 500 m/min. The Edward–Vilgis model fit to the LOY master curve is also shown.

It is apparent from Fig. 15 that the FDY yarns show considerably stiffer behaviour than the LOY master curve. In order to quantify the observed increase in strain hardening, we have fitted the Edwards–Vilgis model to the set of FDY curves by letting the network modulus free, but leaving the yield stress and the extensibility parameter unchanged. The result of this is illustrated in Fig. 16. From this figure, one can clearly see that the FDY curves up to a draw ratio of about 4.4 basically pertain to the same network, which is however stiffer than the network present in the LOY yarn (network modulus of 14.7 MPa as compared to 11.62 MPa for the LOY master curve). FDY yarns produced at a draw ratio higher than 4.4 systematically fall below the fitted curve. This could well be due to the fact that with further extension more and more elements of the network get overstretched and fail, thereby reducing the network density.

The increased network modulus of the FDY yarns could well be due to increased crystallinity in the hot-drawn yarns compared to the LOY yarns. Fig. 17 shows the crystallinities of the studied PA4,6 LOY and FDY yarns obtained by density measurements. All LOY yarns, irrespective of take-up speed have about the same crystallinity around 72%. The hot drawn FDY yarns however, consistently have about 10% higher volume crystallinity (around 80%). This is equivalent to a decrease in the amorphous volume fraction from about 28 vol% for the LOY to about 20 vol% for the FDY.

One can now speculate on how the additional crystallinity stiffens the network. In a zero order approach, we consider two extreme situations here. The first is to assume that the crystals form the network nodes and that these crystals extend laterally to account for the increase in density, thereby consuming amorphous chain segments from the ends of the rubber network chains. In this way the chains that connect the network nodes get about 20/28 (vol%/vol%) shorter. This scenario is

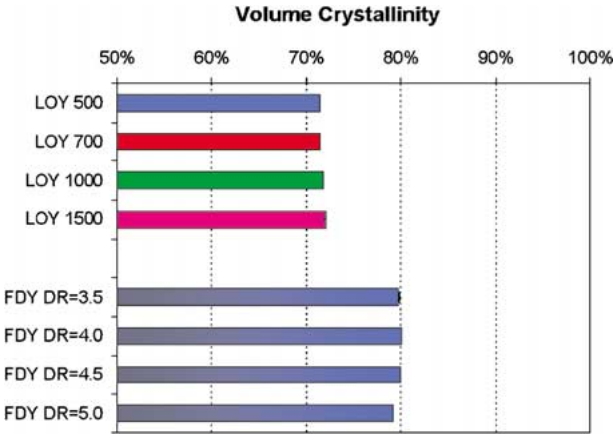

Figure 17 Volume crystallinites of LOY and FDY yarns, obtained by density gradient method.

1. Extended Crystals:
   - Number of network crosslinks is constant
   - Additional crystallinity due to longitudinal growth of the crystals that constitute the network nodes. Chains between the crosslinks get shorter from the ends.
   - $G_{EC} = G_{LOY} * f_{a,LOY} / f_{a,FDY} = 11.62$ MPa * 28% / 20%

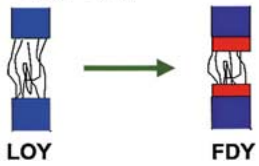

Figure 18 Extended crystal scenario to explain the observed stiffer network behaviour of the FDY yarns.

2. Intermediate layer:
   - Additional crystallinity due to growth of the crystals intermediate to existing network nodes. Chains between the crosslinks get shorter from the middle.
   - $G_{IL} = 2 * G_{LOY} * f_{a,LOY} / f_{a,FDY}$
     $= 2 * 11.62$MPa * 28% / 20%

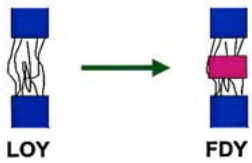

Figure 19 Intermediate layer scenario to explain the observed stiffer network behaviour of the FDY yarns.

illustrated in Fig. 18 and represented by the "Extended crystal" sketch and curve.

The other scenario is that the additional crystallinity in the FDY yarns form new network nodes, which stiffen the network. If one assumes that on average these crystals form halfway the rubbery chains that connect the nodes, then in addition to shortening by a ratio of 20/28, they now also are halved in length. This scenario is represented in Fig. 19 as "Intermediate layer". Since the network modulus is inversely proportional to the internode chain length one can estimate the corresponding network modulus as being doubled. In this coarse comparison one clearly sees that the intermediate layer case is highly unlikely, since it would involve excessive stiffening. The extended crystal scenario is much more likely; actually it fits remarkably well as can be seen from the fitting results of Fig. 20.

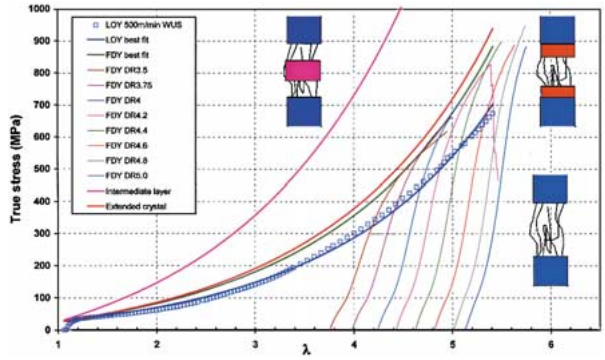

Figure 20 Edwards–Vilgis model predictions on the basis of the Extended crystal and Intermediate layer scenario to explain the observed stiffer network behaviour of the FDY yarns.

4. Conclusions

The mechanical properties of Stanyl® PA4,6 yarns of different take-up speed and draw ratio have been discussed in terms of a molecular network deformation model. It has been shown that, to a first approximation, the network within the PA4,6 yarns retains its nature during the course of different processing steps, such as spinning at different take-up speeds, and cold or hot-drawing. Indeed, true stress–true strain tensile curves of yarns from different origin can be shifted along the strain axis to form a master curve, representative of the yarn's mechanical behaviour. The extent of shift needed is indicative of the degree of orientation experienced by the network during the previous processing steps.

This behaviour is similar to what has been observed for PET fibres [1–4, 6]. In contrast, birefringence in the PA4,6 yarns develops rather quickly with take-up speed, and conforms very well to a pseudo-affine deformation scheme. This pseudo-affine orientation behaviour may well be related to the high degree of volume crystallinity in the PA4,6 yarns as–spun, which is little over 70%.

Analysis of the strain hardening behaviour of the as-spun yarns using rubber elastic models based on sliplink contributions allows to assess important features of the network topology. The descriptions due to Ball–Doi–Edwards and Warner, and to Edwards–Vilgis both perform well as analytical tools. The Edwards-Vilgis model especially gives an excellent description of the mechanical behaviour of the as-spun yarns over a wide draw ratio range. The modelling results moreover indicate that significant sliplink contribution to the deformation does not occur, probably because of fixed crystal behaviour of PA4,6 upon deformation. The, from a physical point of view, unrealisticly short chain length between network nodes has been rationalised by pointing at the strain concentration in the amorphous phase due to non zero dimensions of the crystals.

The tensile true stress–true strain curves of hot-drawn yarns indicate that, to zero order, the network topology remains fairly constant during hot drawing. Although apparent draw ratios, obtained by matching hot-drawn yarns with the LOY master curve, are close to the applied draw ratios, the FDY yarn network consistently shows more strain hardening than the LOY network. This stiffer behaviour is explained by additional

crystallisation during hot-drawing (up to 80% volume crystallinity), whereby it is made plausible that additional crystallinity is mainly due to longitudinal growth of existing crystals, and not to formation of extra fixed crystal links.

Finally it has been demonstrated that the true stress–true strain curve of LOY yarns is very useful in predicting drawability and mechanical properties of the FDY yarns, subsequently drawn from them. This makes true stress–true strain testing of LOY yarns a powerful tool for expedient optimisation of spinning conditions.

Acknowledgements

Prof. Ian Ward, Univ. of Leeds, and Mike Walker and Stuart Krog from SANS, Cape Town are gratefully acknowledged for their helpful comments and suggestions.

References

1. P. R. PINNOCK and I. M. WARD, *Trans. Faraday Soc.* **62** (1966) 1038.
2. S. W. ALLISON, P. R. PINNOCK and I. M. WARD, *Polymer* **7** (1966) 66.
3. S. D. LONG and I. M. WARD, *J. Appl. Pol. Sci.* **42**(7) (1991) 1911.
4. *Idem.*, *ibid.* **42**(7) (1991) 1921.
5. H. M. HEUVEL and R. HUISMAN, *J. Appl. Polym. Sci.* **22** (1978) 2229.
6. H. SHIRATAKI, A. NAKASHIMA, K. SATO and K. OKAJIMA, *ibid.* **64**(13) (1997) 2631
7. H. BRODY, *J. Macromol. Sci. & Phys.* **B22**(1) (1983) 19.
8. K. KOYAMA, J. SURYADEVARA and J. SPRUIELL, *J. Appl. Pol. Sci.* **31**(7) (1986) 2203.
9. W. KUHN, *Kolloidzschr.* **76** (1936) 258.
10. H. M. JAMES and E. GUTH, *J. Chem. Phys.* **15** (1947) 699.
11. R. C. BALL, M. DOI, S. F. EDWARDS and M. WARNER, *Polymer* **22** (1981) 1010.
12. S. F. EDWARDS and TH. VILGIS, *Polymer* **27** (1986) 483.
13. W. G. HU and K. SCHMIDT-ROHR, *Acta Polymerica* **50** (1999) 271.
14. I. M. WARD, "Structure and Properties of Oriented Polymers" (Chapman & Hall, London, 1997) p. 37.
15. J. F. HOTTER, J. A. CUCULO, P. A. TUCKER and B. K. ANNIS, *J. Appl. Pol. Sci.* **69**(11) (1998) 2115.
16. L. R. G. TRELOAR, "The Physics of Rubber Elasticity" (Clarendon, Oxford, 1975).

Received 19 September
and accepted 23 November 2000